

# Modified $GW$ Method in Electronic Systems

Zhipeng Sun,<sup>1,2</sup> Zhenhao Fan,<sup>1,2</sup> Hui Li,<sup>1,2</sup> Dingping Li,<sup>1,2,\*</sup> and Baruch Rosenstein<sup>3,†</sup>

<sup>1</sup>*School of Physics, Peking University, Beijing 100871, China*

<sup>2</sup>*Collaborative Innovation Center of Quantum Matter, Beijing, China*

<sup>3</sup>*Electrophysics Department, National Yang Ming Chiao Tung University, Hsinchu 30050, Taiwan, R. O. C*

A modified  $GW$  approximation to many - body systems is developed. The approximation has the same computational complexity as the traditional  $GW$  approach, but uses a different truncation scheme. This scheme neglects the high order connected correlation functions. A covariant (preserving the Ward identities due to the charge conservation) scheme for the two - body correlators is employed, which holds the relation between the charge correlator and the charge susceptibility. The method is tested on the two - dimensional one - band Hubbard model. The results are compared with exact diagonalization, the  $GW$  approximation, the fluctuation - exchange (FLEX) theory and determinantal Monte Carlo (MC) approach. The comparison for the (one - body) Green's function demonstrates that it is more precise in strong - coupling regime (especially away from half - filling) than the  $GW$  and FLEX approximations, which have a similar complexity. More importantly, this method indicates a Mott - Hubbard gap as the Hubbard  $U$  increases, whereas the  $GW$  and FLEX methods fail. Besides, the charge correlator obtained from the covariant scheme not only holds the consistency of the static charge susceptibility, but also makes a significant improvement over the RPA calculations.

## I. INTRODUCTION

Understanding of physics of the strongly correlated electronic systems has been a challenge in condensed matter theory for many decades. These systems are hosts of distinct phenomena such as the Mott insulator [1], quantum magnetism [2], pseudogap [3], strange metal [4] and  $d$ -wave high-temperature superconductivity [5, 6], all of which cannot be explained within the framework of the traditional renormalized weak coupling expansion. Above the atomic level (described by the density functional approximation), the main features of these systems are typically captured sufficiently well by the lattice effective Hamiltonian with (quasi) local Coulomb repulsion. Up to now, numerous non - perturbative numerical and analytic approaches have been developed to tackle these seemingly simple models, such as the (one or multi - band) Hubbard model [7].

Numerical non - perturbative methods include the density matrix renormalization group (DMRG) [8], determinantal quantum Monte Carlo (MC) simulation [9] and dynamic mean-field theory (DMFT) [10, 11]. They can produce reliable results in certain cases, but have limitations in the cases of interest, for example, at very low temperature or deviations from half filling (doping). DMRG is reliable mostly in one - dimensional case, while the determinantal MC encounters a severe fermionic sign problem and thus fails at low temperature and significant doping. DMFT although successful at intermediate coupling generally misses nonlocal fluctuations. A lot of effort was made to remedy this by the extensions of a more elaborate scheme [12, 13].

Analytic non - perturbative methods evolved from simple mean field methods [2] like variations of Hartree - Fock(HF), to more sophisticated field theoretical methods. Generally, a closed set of (quite complicated) equations of the correlators and the vertex functions is constructed and subsequently solved numerically. Most used approximations are based on the Baym-Kadanoff formalism [14, 15], the Hedin's equations [16], the diagrammatic analysis [17]. Others are based on particular truncations of Dyson - Schwinger equations [18-20].

By their complexity the analytic methods can be broadly classified into two classes. In the simpler class, one identifies a function (or functions) of just *one* energy-momentum variable as the relevant "degrees of freedom". Examples include the electronic Green's function  $G(\omega, k)$ , the screened dynamical potential  $W(\omega, k)$  and the charge and spin susceptibilities  $\chi(\omega, k)$ . Beyond the HF, two popular approximations of this class are the  $GW$  approximation [16, 21], involving  $G$  and  $W$ , and the fluctuation - exchange (FLEX) theory [22], involving  $G$  and  $\chi$ 's. More complicated schemes such as the parquet approximation [23, 24] and covariant quartic approximation [25], in addition to the one - momentum functions, unfortunately have to consider *multiple* - momenta - dependent quantities, such as the two - body vertex functions and the high - order correlators.

---

\* lidp@pku.edu.cn

† vortexbar@yahoo.com

To describe realistic correlated materials, the complicated schemes are often not feasible yet due to their large computational complexity, and thus the simpler class is more favored. However, the current  $GW$  and FLEX approximation produce less accurate data compared with experimental [26] or numerically exact results [24]. Therefore, a simpler yet sufficiently reliable and precise method is highly sought for.

In this paper, one such method, a modification of  $GW$  approximation, is developed. To fully take advantage of the clustering properties of the connected correlators, the modified  $GW$  approximation is to truncating high order connected correlators on the Dyson - Schwinger equations. The resulting equations turn out be quite similar to the  $GW$  equations, and the physical meanings are also analogous. As in  $GW$  the Coulomb interaction is renormalized, the screening for long range interaction is included within the modified  $GW$  approximation. In this degree, this method is applicable to realistic materials.

In a many - body system, the charge conservation leads to a set of the Ward identities. In an approximation (such as  $GW$  or FLEX), the Ward identity for one - body Green's function is obeyed, whereas the Ward identity for the two - body correlator (directly obtained from equations after the approximation) is often violated. Besides, the relation between the charge correlator and charge susceptibility,  $\partial n/\partial\mu = \chi^{\text{ch}}(\omega = 0, k = 0)$ , is often violated [27]. To preserve these identities, the covariant scheme [28-30] is employed in this paper.

The modified  $GW$  approximation is tested on the two - dimensional (2D) one - band Hubbard model in this paper. The results for the density and the Green's function demonstrate that the modified  $GW$  approximation produce satisfactory results *even in strong - coupling regime*, compared with exact diagonalization (ED) or determinantal MC approach. The method also indicates a Mott - Hubbard gap as the Hubbard  $U$  increases, whereas the  $GW$  and FLEX methods fail. The results of charge correlator demonstrate a significant improvement over the RPA scheme, and the charge susceptibility obtained from the covariant scheme is consistent with an independent calculation  $\partial n/\partial\mu$ .

This paper is organized as follows. In Sec. II the modified  $GW$  approximation is presented for the fermionic (one - body) Green's function. Next in Sec. III the covariant scheme for the two - body correlators is presented. And then in Sec. IV this method is tested on the 2D Hubbard model by comparing the (one - body) Green's function (and the density), and the (two - body) charge correlator (and the static charge susceptibility) with other approaches. The conclusions and discussions are given in Sec. V.

## II. MODIFIED $GW$ APPROXIMATION FOR FERMIONIC GREEN'S FUNCTION

In this section, basic equations and assumptions of the modified  $GW$  approximation are presented. The general density - density type interacting fermionic system at finite temperature is considered. Two exact equations involving the connected correlators are derived. The approximation is motivated by the clustering properties of the connected correlators.

### A. Two exact equations for correlators

The Matsubara action for a density - density type interacting fermionic system at finite temperature has the form

$$S[\psi, \psi^*] = - \int d(12) T(1, 2) \psi^*(1) \psi(2) + \frac{1}{2} \int d(12) V(1, 2) \rho(1) \rho(2), \quad (1)$$

where  $\psi^*$ ,  $\psi$  are Grassmannian fields and  $\rho(1) \equiv \psi^*(1) \psi(1)$  is the density (composite operator). The label  $(1) \equiv (\sigma_1, x_1, \tau_1)$  represents a generalized coordinate, containing the spin projection  $\sigma_1$ , the space coordinate  $x_1$ , and the Matsubara time  $0 < \tau_1 < \beta$ , with  $\beta$  being the inverse temperature. The condensed notation  $\int d(1)$  stands for the integral or summation over all the values of a generalized coordinate  $(\sigma_1, x_1, \tau_1)$ . The bi - local functions  $T$  and  $V$  are the hopping strength and the interaction (dynamical) "potential". Generalization to several fermionic species or type of interactions (spin, current) is straightforward.

Consider the perturbation of the system by an external bosonic source  $\phi(1)$  (local spin selective chemical potential) coupled to the density :

$$S[\psi, \psi^*; \phi] = S[\psi, \psi^*] - \int d(1) \phi(1) \rho(1). \quad (2)$$

Note that unlike in [25], the source is coupled to a quantity quadratic in the fermionic fields. Using the grand

partition function,

$$Z[\phi] = \int \mathcal{D}[\psi, \psi^*] e^{-S[\psi, \psi^*; \phi]}, \quad (3)$$

the (one - body) Green's function  $G$  is given by:

$$G(1, 2) \equiv \langle \psi^*(2) \psi(1) \rangle = \frac{1}{Z[\phi]} \int \mathcal{D}[\psi, \psi^*] \psi^*(2) \psi(1) e^{-S[\psi, \psi^*; \phi]}. \quad (4)$$

Here  $\int \mathcal{D}[\psi, \psi^*]$  is the (Grassmannian) functional path integral measure.

The Green's function  $G(1, 2)$  and its functional derivative  $\delta G(1, 2)/\delta\phi(3)$  are related through the following equation of motion (see Appendix A 1, for derivation):

$$\delta(1, 2) = \int d(3) H^{-1}(1, 3) G(3, 2) - \int d(3) V(1, 3) \frac{\delta G(1, 2)}{\delta\phi(3)}. \quad (5)$$

Here  $\delta(1, 2)$  is the Dirac/Kronecker delta function and the ‘‘Hartree’’ propagator  $H$  is defined by

$$H^{-1}(1, 2) \equiv T(1, 2) + \delta(1, 2) v(1). \quad (6)$$

Here the density weighted interaction potential  $v$  is:

$$v(1) \equiv \phi(1) - \int d(2) V(1, 2) \rho(2). \quad (7)$$

Note that in the absence of the external source, i.e.  $\phi = 0$ , the quantity  $H$  is the free Green function with Hartree self - energy absorbed in the chemical potential.

Functional derivative of Eq.(5) with respect to the source  $\phi$  yields,

$$\begin{aligned} 0 = & \int d(4) \frac{\delta H^{-1}(1, 4)}{\delta\phi(3)} G(4, 2) + \int d(4) H^{-1}(1, 4) \frac{\delta G(4, 2)}{\delta\phi(3)} \\ & - \int d(4) V(1, 4) \frac{\delta^2 G(1, 2)}{\delta\phi(3) \delta\phi(4)}, \end{aligned} \quad (8)$$

relating the one - body correlator  $G$  and the two - body correlator  $\delta G/\delta\phi$  to the three - body correlator  $\delta^2 G/\delta\phi^2$ . By successive functional derivatives, one can obtain a hierarchy of such relations for even higher order correlators. These are used in the search of successful non - perturbative approximations by truncating certain terms considered small by a certain qualitative argument valid for a particular class of systems and values of parameters. This way a closed set of equations obtained and solved numerically typically by iterations.

## B. Clustering property of connected correlators and the $HGW$ truncation

The simplest approximation is to truncating  $\delta G/\delta\phi$  in the first equation of motion Eq.(5). This yields  $G = H$ , namely the Hartree approximation widely used in condensed matter physics [2]. A more complicated (and hopefully precise, see below) approximation would be truncating the  $\delta^2 G/\delta\phi^2$  term in Eq.(8). Justification for such a truncation originates from the clustering property, which states that the connected correlation function is very small as its coordinates are separated. The quantity

$$\frac{\delta^2 G(1, 2)}{\delta\phi(3) \delta\phi(4)} = \langle \psi^*(2) \psi(1) \rho(3) \rho(4) \rangle_c \quad (9)$$

is a connected correlation function, and thus can be omitted in certain cases. The reliability of this truncation is determined by the inequality

$$\left| \int d(45) H(1, 5) V(5, 4) \frac{\delta^2 G(1, 2)}{\delta\phi(3) \delta\phi(4)} \right| \ll \left| \int d(45) H(1, 4) \frac{\delta H^{-1}(4, 5)}{\delta\phi(3)} G(5, 2) \right|. \quad (10)$$

Then one can approximate Eq.(8) by

$$\frac{\delta G(1, 2)}{\delta\phi(3)} = - \int d(45) H(1, 4) \frac{\delta H^{-1}(4, 5)}{\delta\phi(3)} G(5, 2). \quad (11)$$

The validity of inequality (10) will be indirectly checked by whether the Green's function obtained within the approximation is in good agreement with the numerically exact results.

Eqs.(5, 11) form a closed set, and will yield the *HGW* equations (for derivation, see Appendix B 1):

$$G^{-1}(1, 2) = H^{-1}(1, 2) - \Sigma(1, 2), \quad (12a)$$

$$\Sigma(1, 2) = -H(1, 2)W(2, 1), \quad (12b)$$

$$W^{-1}(1, 2) = V^{-1}(1, 2) - \Pi(1, 2), \quad (12c)$$

$$\Pi(1, 2) = H(1, 2)G(2, 1). \quad (12d)$$

Apparently, these equations resemble those of the *GW* approximation (see Ref.[21] or appendix F). The equations Eq.(12a) for Green's function  $G$  and Eq.(12c) for screened dynamical potential  $W$  are the same, whereas the equations Eq.(12b) for self energy function  $\Sigma$  and Eq.(12d) for polarization function  $\Pi$  are different. The *HGW* approximation is named due to its similarity to the *GW* approximation and Hartree approximation. Some of the propagators  $G$  in *GW* equations are replaced by the Hartree propagator  $H$  in the *HGW* equations.

Essentially, the *HGW* equations and *GW* equations are based on different approximation schemes. The *HGW* equations are derived by the truncation of high order connected correlators, whereas the *GW* equations are based on simplification of Hedin's vertex. The comparison of these two sets of equations is summarized in Table I.

TABLE I. Comparison between the *HGW* and *GW* equations

	<i>HGW</i>	<i>GW</i>
Equation for $G$	$G^{-1} = H^{-1} - \Sigma$	
Equation for $\Sigma$	$\Sigma = -HW$	$\Sigma = -GW$
Equation for $W$	$W^{-1} = V^{-1} - \Pi$	
Equation for $\Pi$	$\Pi = HG$	$\Pi = GG$
Approximation	$\delta^2 G / \delta \phi^2 = 0$	$\Lambda = \hat{1}$

These formulas will be used to calculate the one - body Green's functions and the particle density in Sec. IV. Now we turn to more complicated many - body correlators.

### III. COVARIANT *HGW* APPROXIMATION FOR THE TWO - BODY CORRELATOR

In this section, the covariant scheme is employed for the two - body correlators within the *HGW* approximation. The covariant *HGW* equations for the density - density correlators are also derived by functional derivatives of the *HGW* equations.

#### A. Ward identities and covariance

In a many - body system, the charge conservation leads to a set of the Ward identities (see Appendix A 2). In an approximation (such as *GW* or FLEX), the Ward identity for one - body Green's function is obeyed, whereas the Ward identity for the two - body correlator (directly obtained from equations after the approximation) is often violated. Besides, the relation between the charge correlator and charge susceptibility,  $\partial n / \partial \mu = \chi^{\text{ch}}(q = 0, \omega = 0)$ , is also often violated. To preserve the consistency in the *HGW* approximation, one can define the two - body (connected) correlator as the functional derivative of Green's function  $G$  with respect to the external source  $\phi$ :

$$L^{\text{cov}}(1, 2; 3) = \left. \frac{\delta G(1, 2)}{\delta \phi(3)} \right|_{\phi=0}. \quad (13)$$

Here  $G$  is obtained from the off - shell (nonzero  $\phi$ ) equations. The superscript "cov" in  $L^{\text{cov}}$  denotes for "covariant".

As  $G$  obeys the Ward identity for all  $\phi$ 's, the derivative of the Ward identity is also satisfied:

$$\int d(2) \left( T(1, 2) \frac{\delta G(2, 1)}{\delta \phi(3)} - T(2, 1) \frac{\delta G(1, 2)}{\delta \phi(3)} \right) = 0. \quad (14)$$

Letting  $\phi = 0$  in Eq.(14), one obtains:

$$\int d(2) (T(1, 2) L^{\text{cov}}(2, 1; 3) - T(2, 1) L^{\text{cov}}(1, 2; 3)) = 0. \quad (15)$$

Thus one arrives at the conclusion that  $L^{\text{cov}}$  defined by Eq.(13) satisfies the Ward identity for the two - body correlator. In other words, the covariant scheme automatically preserves all the charge - conserving laws.

### B. Covariant $HGW$ equations for the density - density correlator

The covariant version of the density - density correlator is defined as,

$$\chi^{\text{cov}}(1, 2) = \left. \frac{\delta \rho(1)}{\delta \phi(2)} \right|_{\phi=0}, \quad (16)$$

with  $\rho$  the density obtained from off - shell  $HGW$  equations Eq.(12). To compute  $\chi^{\text{cov}}$ , one differentiates the  $HGW$  equations with respect to  $\phi$ . After calculation, given in Appendix B 2, one obtains

$$\chi^{\text{cov}}(1, 2) = \chi_0(1, 2) - \int d(34) \chi_0(1, 3) V(3, 4) \chi^{\text{cov}}(4, 2), \quad (17)$$

where the covariant version of polarization function  $\chi_0$  satisfies the equation:

$$\chi_0(1, 2) = - \int d(34) G(1, 3) G(4, 1) \Lambda(3, 4; 2). \quad (18)$$

The covariant version of vertex function  $\Lambda$  satisfies a set of linear equations (B18, B19) given in Appendix B 2.

The calculation procedure for  $\chi^{\text{cov}}$  in the covariant  $HGW$  approximation therefore can be summarized as follows. First, one solves the on - shell ( $\phi = 0$ )  $HGW$  equations (12) to obtain  $H, G, W$ . Second, one solves Eqs.(B18, B19) to obtain  $\Lambda$ . Third, one uses Eq.(18) to calculate  $\chi_0$ . Finally, one solves Eq.(17) to obtain  $\chi^{\text{cov}}$ . These equations, Eqs.(B18, B19, 18, 17), are referred to the covariant  $HGW$  equations.

Let us contrast this with frequently used RPA formula for  $\chi$ ,

$$\chi^{\text{RPA}}(1, 2) = \bar{\chi}(1, 2) - \int d(34) \bar{\chi}(1, 3) V(3, 4) \chi^{\text{RPA}}(4, 2), \quad (19)$$

where the Lindhard polarization function  $\bar{\chi}$  is given by

$$\bar{\chi}(1, 2) = -G(1, 2) G(2, 1), \quad (20)$$

with  $G(1, 2)$  approximated within a certain approach (such as the  $GW$ ). Although the RPA scheme is much simpler than the covariant scheme, it does not guarantee the Ward identities. Besides, the charge susceptibility (charge susceptibility)  $\partial n / \partial \mu$  is not consistent with that obtained from the RPA calculation [27]. In contrast, the covariant scheme preserves all these identities.

## IV. COMPARISON WITH OTHER APPROXIMATIONS IN THE 2D HUBBARD MODEL

In this section the  $HGW$  approximation is tested on a (numerically) solvable model, the 2D one - band Hubbard model. Exact diagonalization is possible on a relatively small cluster  $N \times N$ ,  $N = 4$ , so we mainly focus on this system. In many cases we use determinantal Monte Carlo (MC) in the range of parameters in which it is consistent with the exact diagonalization (practically not too low temperature and not too large  $U$ ).

The discretized time Matsubara action is employed for numerical implementation to the 2D Hubbard model. Results of the Green's function (and the density) within the  $HGW$  approximation and the charge correlator (and charge susceptibility) based on the covariant scheme are presented. At any stage the  $HGW$  method is compared to two other relatively simple analytic approaches,  $GW$  and FLEX (generally all the three approximations are much better than the Hartree - Fock approximation not shown here).

### A. Matsubara action for the 2D Hubbard model

The Hamiltonian of the 2D Hubbard model is:

$$\hat{\mathcal{H}} = \sum_{ij} \sum_{\sigma=\uparrow, \downarrow} t_{ij} \hat{\psi}_{i, \sigma}^\dagger \hat{\psi}_{j, \sigma} + U \sum_i \hat{\psi}_{i \uparrow}^\dagger \hat{\psi}_{i \uparrow} \hat{\psi}_{i \downarrow}^\dagger \hat{\psi}_{i \downarrow} - \mu \sum_{i, \sigma} \hat{\psi}_{i, \sigma}^\dagger \hat{\psi}_{i, \sigma}. \quad (21)$$

Here  $\hat{\psi}_{i\sigma}^\dagger, \hat{\psi}_{i\sigma}$  are the creation and annihilation operators of electron with spin  $\sigma = \uparrow, \downarrow$  on lattice site  $i$ . The labels  $i, j$  denote the coordinates on the  $N \times N$  2D square lattice with periodic boundary conditions (and lattice constant setting the unit of length). The hopping strength  $t_{ij}$  equals to  $-t$ , if sites  $i, j$  are nearest neighbors and 0 otherwise. We set  $t = 1$  to the unit of energy. Coupling  $U$  is the on - site repulsion, and  $\mu$  is the chemical potential.

The discretized time Matsubara action [31] for Hamiltonian (21) has the form:

$$S_M[\psi, \psi^*] = \sum_{l=0}^{M-1} \sum_{\sigma=\uparrow, \downarrow} \sum_i \psi_{i\sigma}^*(\tau_l) (\psi_{i\sigma}(\tau_{l+1}) - \psi_{i\sigma}(\tau_l)) + \Delta\tau \sum_{l=0}^{M-1} \mathcal{H}[\psi_{i\sigma}^*(\tau_l), \psi_{i\sigma}(\tau_l)]. \quad (22)$$

Here  $M$  is the number of Matsubara time slices, so that  $\Delta\tau \equiv \beta/M$  is the time step. The discrete label  $l$  takes integral value in  $[0, M-1]$  and  $\tau_l \equiv l\Delta\tau$ . The functional  $\mathcal{H}$  is obtained by substituting  $\psi_{i\sigma}^*(\tau_l), \psi_{i\sigma}(\tau_l)$  for  $\hat{\psi}_{i\sigma}^\dagger, \hat{\psi}_{i\sigma}$  in Hamiltonian  $\hat{\mathcal{H}}$  respectively.

Comparing the Matsubara action (22) with general action (1), and one obtains the expression for the hopping matrix  $T$ :

$$T(1, 2) = \Delta\tau \delta_{\sigma_1\sigma_2} \left( -\frac{1}{\Delta\tau} \delta_{i_1i_2} (\delta_{l_1, l_2-1} - \delta_{l_1, l_2}) - t_{i_1i_2} \delta_{l_1l_2} + \mu \delta_{i_1i_2} \delta_{l_1l_2} \right), \quad (23)$$

and expression for the two - body interaction potential  $V$ :

$$V(1, 2) = \Delta\tau U (1 - \delta_{\sigma_1\sigma_2}) \delta_{l_1l_2} \delta_{i_1i_2}, \quad (24)$$

where (1) denotes  $(\sigma_1, i_1, \tau_1)$ , which is a collection of the spin, Matsubara time, and lattice coordinate indexes. The correlators in discretized time Matsubara action are discussed in Appendix D.

For a given set of parameters  $U, \mu, T \equiv 1/\beta$  (and  $N, M$ ), one solves the *HGW* equations Eq.(12) to obtain the Green's functions. The *HGW* equations in frequency - momentum space is given in Appendix C 2, the covariant *HGW* equations in frequency - momentum space is given in Appendix C 3, and the numerical algorithm and cost are described in Appendix E. We start with the thermodynamics and then proceed to the Matsubara Green's function and the charge correlator.

## B. Doping dependence of the particle density

To study the doping dependence of the particle density we chose  $T = 0.125$  for  $4 \times 4$  cluster and two values of the on - site repulsion  $U = 2$ , representing the weak coupling strength, see Fig.1(a) and  $U = 4$ , representing the intermediate coupling strength, see Fig.1(b). The results are compared with those obtained from *GW*, *FLEX* and determinantal MC (the ED approach produces the numerically same results). In Fig.1(a), the three curves are all close to MC result (dots), which means *HGW*, *GW* and *FLEX* all produce satisfactory results of the density at weak coupling regime. In Fig.1(b), the *HGW* curve is much closer to MC result than *GW* and *FLEX* when the particle density is larger than 0.6, which shows *HGW* is much better than *GW* and *FLEX* in the strong antiferromagnetic fluctuation regime. Besides, MC dots show a plateau resembling for the Mott - Hubbard gap (due to the strong antiferromagnetic fluctuation) phase near half filling. The *HGW* curve exhibits this property, whereas *GW* and *FLEX* fails. In this degree, the *HGW* approximation has advantage in capturing the Mott - Hubbard gap over *GW* and *FLEX* approximation.

## C. Matsubara Green's function

### 1. Matsubara Green's function at the Matsubara time axis

We compare results of Green's function at the Matsubara time axis at the anti - nodal momentum  $k = (\pi, 0)$  and the nodal point  $k = (\pi/2, \pi/2)$  (see Fig.2) for different doping and the coupling strength with  $T = 0.125$  for the  $4 \times 4$  cluster. At  $U = 2$  and half - filling (see Fig.2(a,e)), the *GW* and *FLEX* curves are close to the MC data (dots), whereas the *HGW* curve is relatively further. At  $U = 2$  and away from half - filling (see Fig.2(b,f)), the three curves are close to each other, but all relatively further away from the MC result. These results demonstrate that *HGW* might not be advantageous in the weak coupling regime (particularly at half - filling).

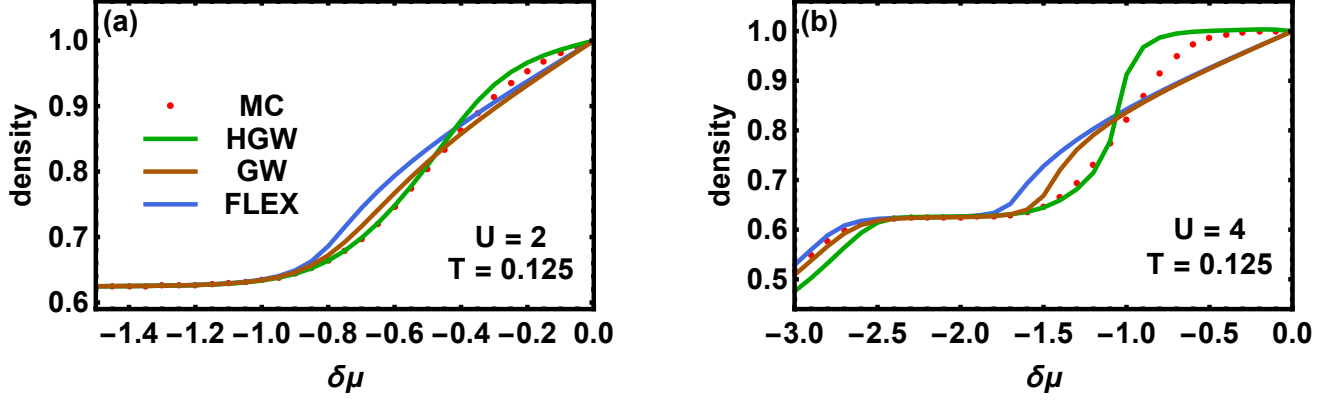


FIG. 1. The doping  $\delta\mu$  dependence of the particle density at (a)  $U = 2, T = 0.125$  and (b)  $U = 4, T = 0.125$  for the  $4 \times 4$  Hubbard cluster. The red dots denote the results obtained from MC. The darker green line denotes the results obtained from *HGW* equations. The darker orange line denotes the results obtained from *GW* equations. The royal blue line denotes the results obtained from *FLEX* approximation.

At a stronger coupling  $U = 4$ , at half - filling (see Fig.2(c,g)), the *HGW* curve is much closer to the MC than the *GW* and the *FLEX* curves. As away from half - filling (see Fig.2(d,h)), the *HGW* curve is also much closer to the MC data than the *GW* and *FLEX* curves. These results demonstrate that, the *HGW* approximation has a considerable advantage over *GW* and *FLEX* in strong coupling regime especially away from half - filling.

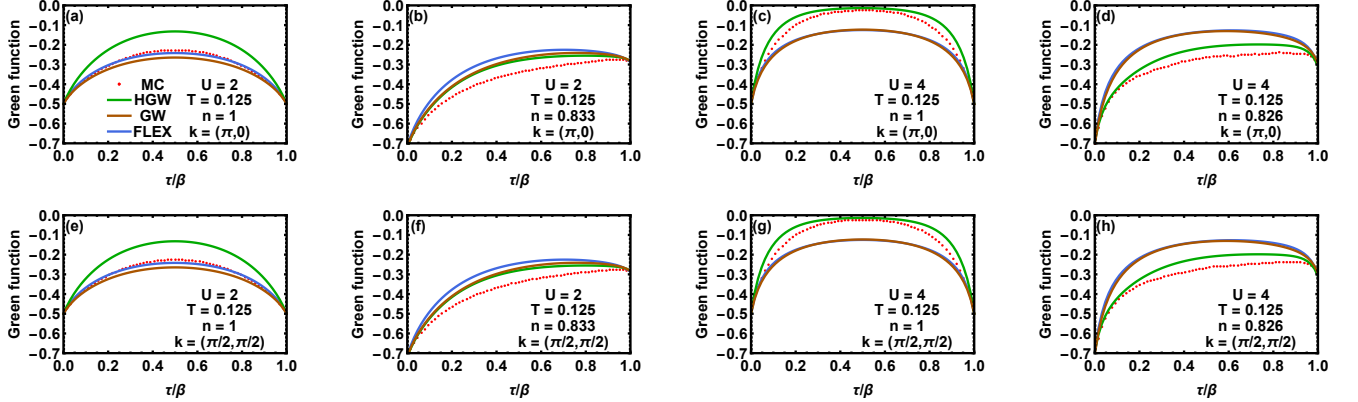


FIG. 2. Comparison of results of Green's function at Matsubara time axis for  $4 \times 4$  cluster at  $T = 0.125$  for different parameters: (a)  $U = 2, n = 1, k = (\pi, 0)$ , (b)  $U = 2, n = 0.833, k = (\pi, 0)$ , (c)  $U = 4, n = 1, k = (\pi, 0)$ , (d)  $U = 4, n = 0.826, k = (\pi, 0)$ , (e)  $U = 2, n = 1, k = (\pi/2, \pi/2)$ , (f)  $U = 2, n = 0.833, k = (\pi/2, \pi/2)$ , (g)  $U = 4, n = 1, k = (\pi/2, \pi/2)$ , (h)  $U = 4, n = 0.826, k = (\pi/2, \pi/2)$ . The red dots denote the results obtained from MC. The darker green line denotes the results obtained from the *HGW* equations. The darker orange line denotes the results obtained from the *GW* equations. Royal blue line denotes the results obtained from the *FLEX* approximation.

At half filling, the determinantal MC is applicable to  $8 \times 8$  lattice. We compare the *HGW* method in these cases (see Fig.3). These results also demonstrate that at  $U = 2$ , the *HGW* method is worse than the *GW* and *FLEX* methods, but is better at  $U = 4$ .

These results can be understood as follows. The *HGW* approximation is obtained by truncating the three - body connected correlators, which have a good clustering property at a stronger coupling  $U$ . At  $U = 2$ , the three - body connected correlators might be very nonlocal and the inequality (10) does not hold, and as a result, the *HGW* method performs not so good. As a contrast, at  $U = 4$ , the connected correlators become local and the *HGW* method exhibits its advantage.

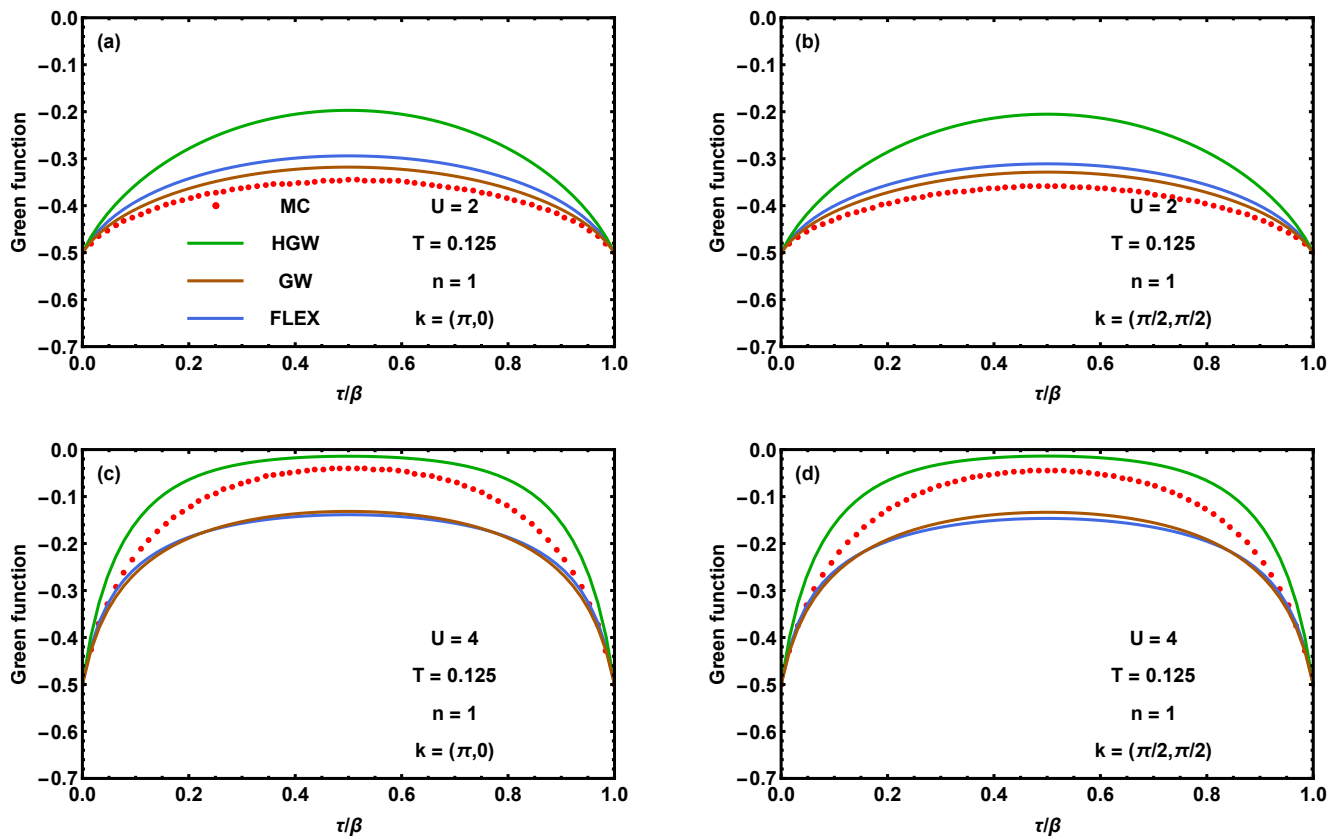


FIG. 3. Comparison of results of Green's function at Matsubara time axis for  $8 \times 8$  cluster for different parameters: (a)  $U = 2, T = 0.125, n = 1, k = (\pi, 0)$ , (b)  $U = 2, T = 0.125, n = 1, k = (\pi/2, \pi/2)$ , (c)  $U = 4, T = 0.125, n = 1, k = (\pi, 0)$ , (d)  $U = 4, T = 0.125, n = 1, k = (\pi/2, \pi/2)$ . The red dots denote the results obtained from determinantal MC. The darker green line denotes the results obtained from *HGW* equations. The darker orange line denotes the results obtained from *GW* equations. The royal blue line denotes the results obtained from *FLEX* approximation.

## 2. Spectral function at half - filling

Using the discrete Fourier transformation, one obtains the values of the Green's function at small Matsubara frequencies from those at Matsubara time axis. The comparison of imaginary part of the value of the Green's function at Matsubara frequency axis at half - filling for  $8 \times 8$  cluster is shown in Fig.4. These results demonstrate again that the *HGW* method is worse than the traditional *GW* method in the weak coupling regime. At a stronger coupling,  $U = 4$ , the shape of the *HGW* curve implies a Mott - Hubbard gap, just like the MC curve. On the contrary, the *GW* method fails.

With the values of the Green's function at some Matsubara frequencies, one can obtain the spectral function by the analytical continuation. We adopt the Nevanlinna analytical continuation[32], which is applicable to noiseless Matsubara data. The results of the spectral function at  $U = 4, T = 0.125$  at half - filling for the  $8 \times 8$  cluster are shown in Fig.5. The spectral function obtained from the *HGW* method does exhibit a Mott - Hubbard gap. The spectral function for 2D half - filling Hubbard model has been studied by various methods, for example, the Monte Carlo simulation[33], the ladder dual fermion approximation[34], the cellular dynamical mean field theory[35], and the cluster perturbation theory[36]. We found that our results are similar to those obtained by the cluster perturbation theory (Fig.9c presented in Ref[34]).

## D. Charge density correlator and charge susceptibility at half filling

We compare the charge correlator in Matsubara time at the quasi - momentum  $(\pi, \pi)$  obtained from the covariant *HGW* approximation (*cHGW*) with those based on the RPA formula (19, 20), where the Green's functions  $G$  obtained from the *HGW*, *GW*, *FLEX* approximations are used.



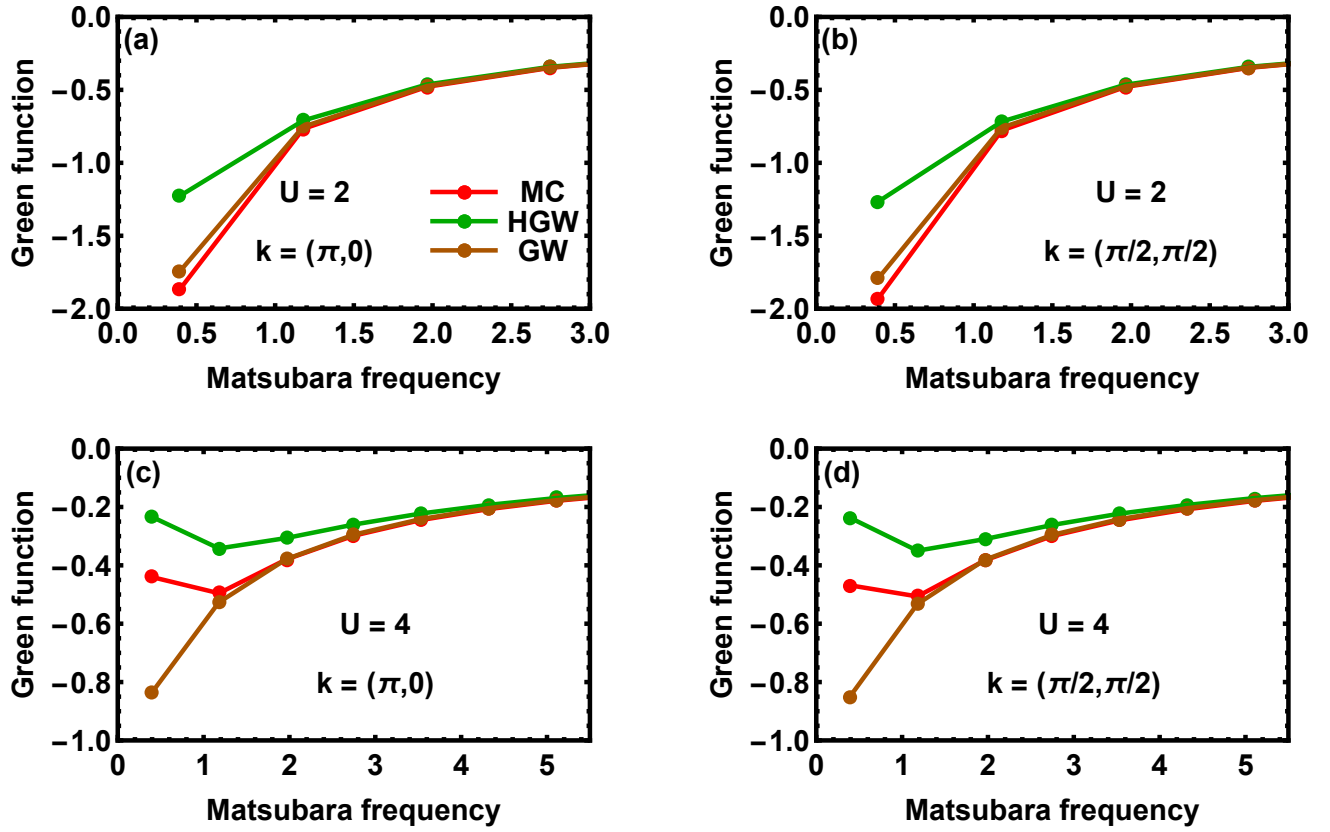


FIG. 4. Comparison of the results of the imaginary part of the Green's function at the Matsubara frequency axis for  $8 \times 8$  cluster for different parameters: (a)  $U = 2, T = 0.125, n = 1, k = (\pi, 0)$ , (b)  $U = 2, T = 0.125, n = 1, k = (\pi/2, \pi/2)$ , (c)  $U = 4, T = 0.125, n = 1, k = (\pi, 0)$ , (d)  $U = 4, T = 0.125, n = 1, k = (\pi/2, \pi/2)$ . The red dots denote the results obtained from determinantal MC. The darker green line denotes the results obtained from *HGW* equations. The darker orange line denotes the results obtained from *GW* equations.

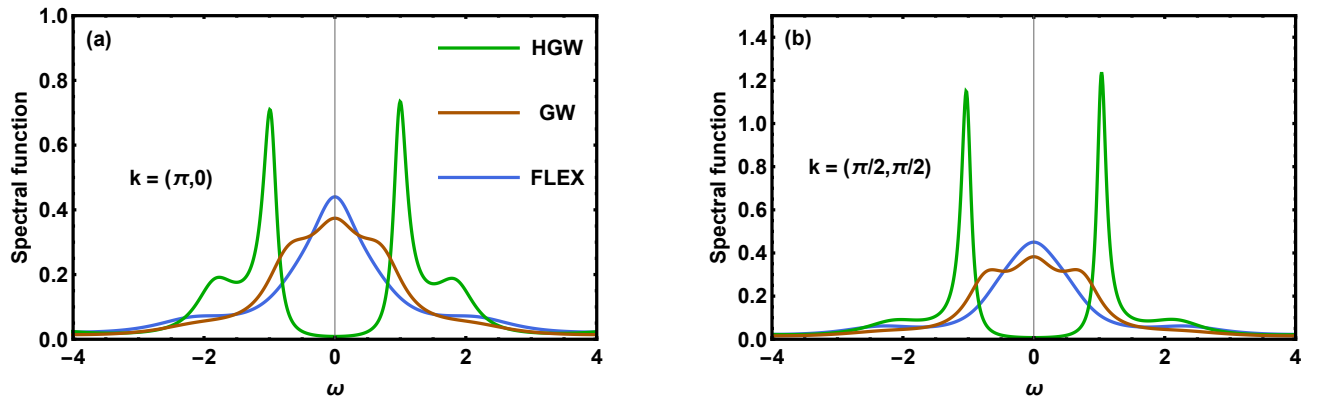


FIG. 5. Comparison of the results of the spectral functions for  $8 \times 8$  cluster at  $U = 4, T = 0.125$  and half-filling at different momenta: (a)  $k = (\pi, 0)$ , (b)  $k = (\pi/2, \pi/2)$ . The darker green line denotes for the results of the spectral function obtained from the *HGW* method, the darker orange line denotes for those obtained from the *GW* method, and the royal blue line denotes for those obtained from the *FLEX* theory.

We study the  $4 \times 4$  cluster and set  $M = 1024$ . Two sets of parameters are chosen:  $U = 2, T = 0.125$  in Figs.6(a, b), and  $U = 4, T = 0.125$  in Figs.6(c, d). Since the results turn out to be too close to differentiate, only the FLEX and MC curves for the charge correlator are plotted in Figs.6(a, c), and the differences between results obtained from the above approximations and those obtained from MC are plotted in Figs.6(b, d).

In Fig.6(b) with parameter  $U = 2, T = 0.125$ , the largest differences given by  $HGW$ ,  $GW$  and FLEX (within the RPA formula) are all about 0.12 (near  $\tau = 0$  and  $\tau = \beta$ ), while that given by  $cHGW$  is about 0.01. In Fig.6(d) with parameter  $U = 4, T = 0.125$ , the largest differences (near  $\tau = 0$  and  $\tau = \beta$ ) given by  $HGW$ ,  $GW$  and FLEX are all about 0.15, while that given by  $cHGW$  is less than 0.01. These results demonstrate that the covariant scheme makes a significant improvement over the RPA calculations.

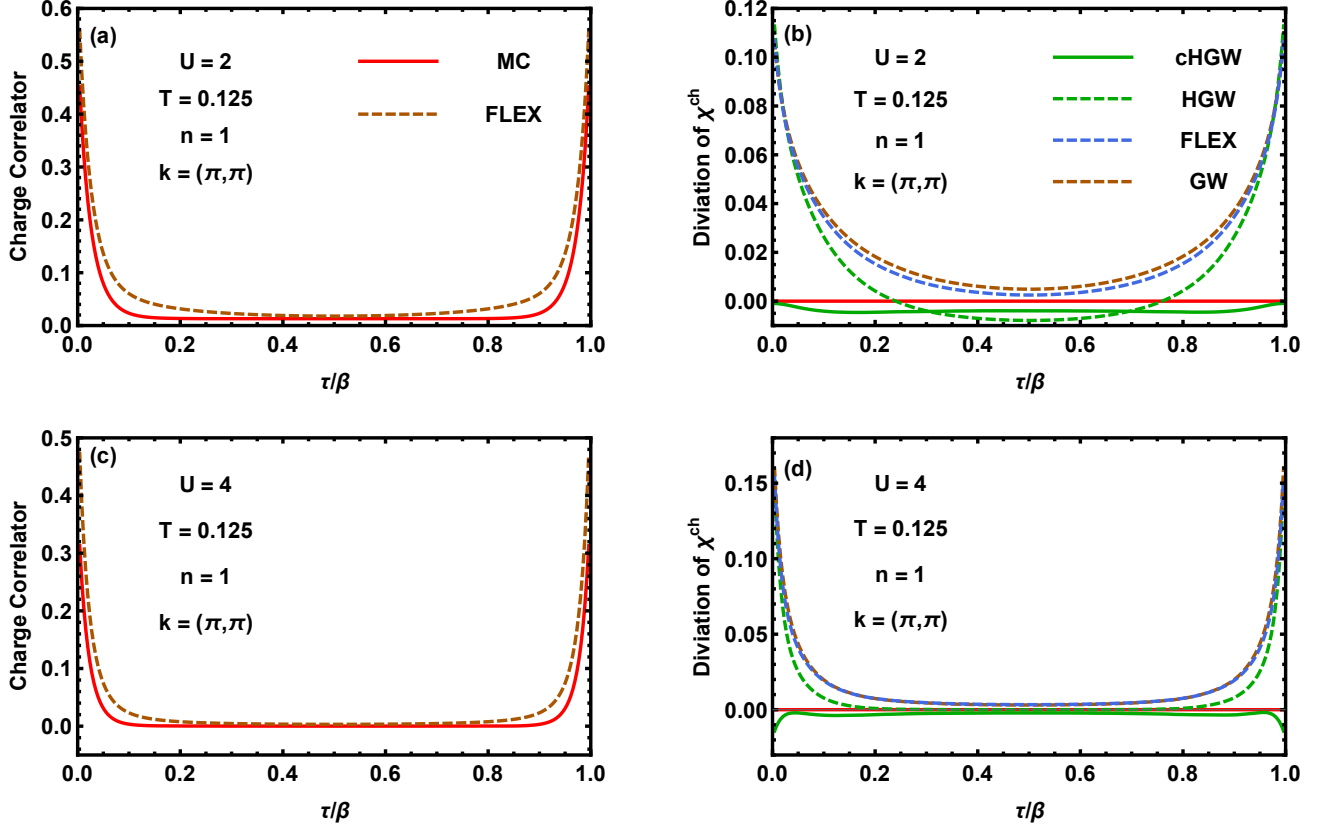


FIG. 6. Comparison of results of charge correlator in Matsubara time at  $k = (\pi, \pi)$  the  $4 \times 4$  Hubbard cluster. For  $U = 2, T = 0.125, n = 1$ , (a) shows the results of charge correlator obtained from FLEX and MC, and (b) shows the differences between results of charge correlator obtained from different approximations and those obtained from MC. For  $U = 4, T = 0.125, n = 1$ , (c) shows the results of charge correlator, and (d) shows the differences. The red line denotes for MC. The darker green solid line denotes for  $cHGW$ , and the darker green dashed line denotes for  $HGW$ . The darker orange dashed line denotes for  $GW$ . The royal blue dashed line denotes for FLEX.

We study the dependence of the static charge susceptibility  $\chi^{\text{ch}}(i\Omega = 0, k)$  on the coupling strength  $U$  at  $T = 0.125$ , and these results are presented in Figs.7(a, b). The curves obtained from the  $cHGW$  method and the RPA calculations with the Green's function obtained from the  $HGW$ ,  $GW$  and FLEX approximations have a similar tendency to the MC curve. The  $cHGW$  curve is much closer to the MC curve, which demonstrates again the covariant scheme makes a significant improvement over the RPA calculations.

We also compare the values of  $\partial n / \partial \mu$  (by variation of the density with the chemical potential, i.e.  $\Delta n / \Delta \mu$ ) at different couplings, and the results are presented in Fig.7(c). The  $HGW$  curve is much closer to the MC curve than the  $GW$  and FLEX curves. The tendency of  $\partial n / \partial \mu$  to 0 as  $U$  increases showed by the MC results demonstrates the Mott - Hubbard gap at strong coupling.

In a self-consistent theory, the static charge susceptibility  $\chi_c \equiv \chi^{\text{ch}}(i\Omega = 0, k = 0)$  is equal to the quantity  $\partial n / \partial \mu$  from an independent calculation. To study this consistency, we compare the quantity  $\partial n / \partial \mu - \chi_c$ , and the results are presented in Fig.7(d). The results demonstrate that the MC and the covariant calculations hold the consistency, whereas the RPA calculations have significant deviations.

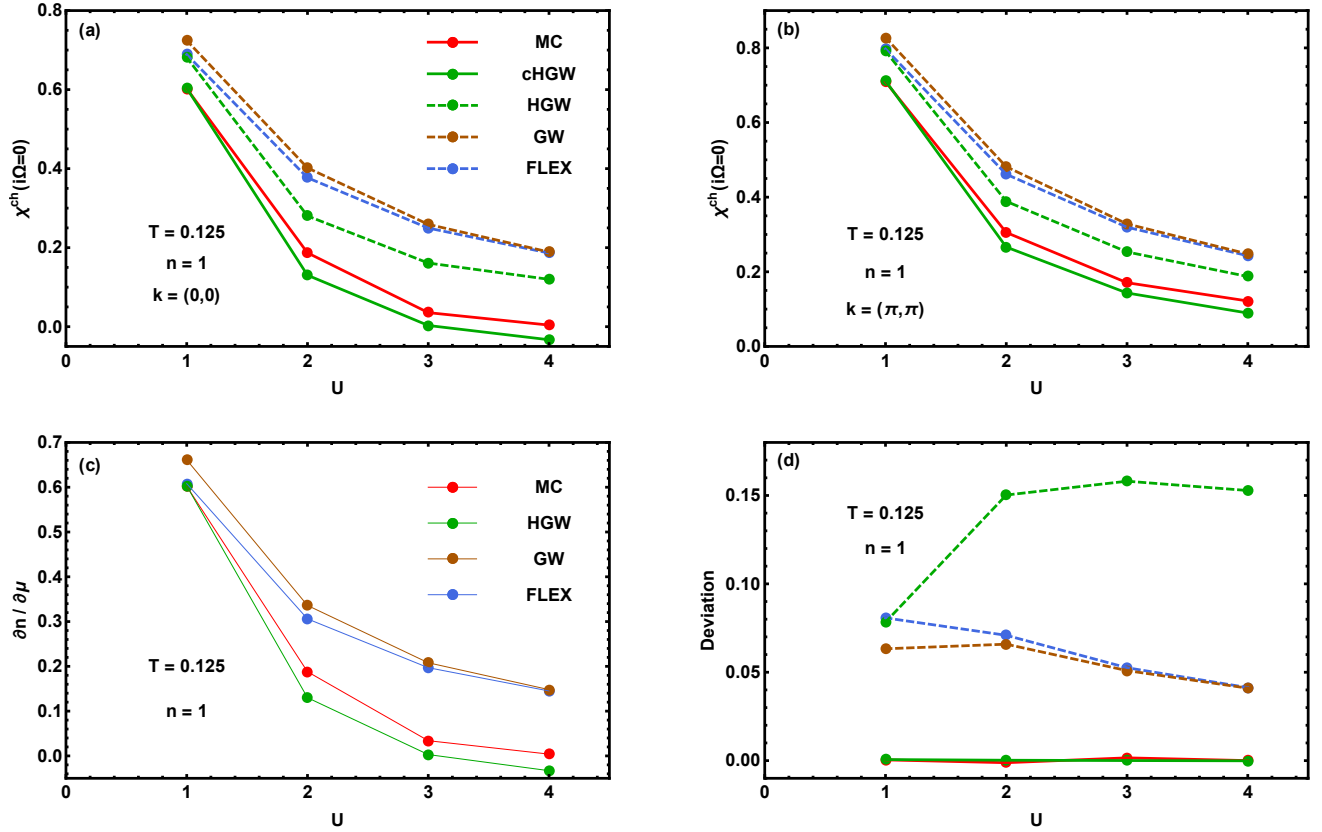


FIG. 7. Comparison of the results of the static charge susceptibility dependence of  $U$  at  $T = 0.125$  for the  $4 \times 4$  Hubbard cluster. (a) shows the results of the static charge susceptibility obtained from the MC,  $cHGW$ ,  $HGW$ ,  $GW$ , FLEX methods, at  $k = (0,0)$ , (b) at  $k = (\pi,\pi)$ . (c) shows the values of  $\partial n / \partial \mu$  obtained from the independent calculations through MC,  $HGW$ ,  $GW$  and FLEX methods. (d) shows the deviation of the RPA calculations. In Figs.(a, b, d), the red line denotes for MC, the darker green solid line denotes for  $cHGW$ , the darker green dashed line denotes for  $HGW$ , the darker orange dashed line denotes for  $GW$ , and the royal blue dashed line denotes for FLEX. In Fig.(c), the red line denotes for MC, the darker green solid line denotes for  $HGW$ , the darker orange solid line denotes for  $GW$ , and the royal blue solid line denotes for FLEX.

## V. CONCLUSION AND DISCUSSION

To summarize, the  $HGW$  approximation, a modified  $GW$  approximation, is developed. It is derived by introduction of an external source  $\phi$  coupled to the density  $\rho$  and truncation of high order correlators on equations of motion. The complexity of the  $HGW$  equations turn out to be very similar to  $GW$  equations. The  $HGW$  approximation is compared with other approximations of comparable complexity  $GW$ , FLEX in the Hubbard model. The results of the density and Green's function demonstrate that the  $HGW$  approximation has a significant advantage over  $GW$  and FLEX in a relative strong coupling regime especially away from half - filling. More importantly, the  $HGW$  approximation exhibits a gap as  $U$  increases, whereas the  $GW$  and FLEX methods fail.

To obtain the charge - conserving two - body correlators in the  $HGW$  approximation, the covariant scheme is developed. In this scheme, the two - body correlators are calculated through functional derivatives of Green's function  $G$  with respect to the source  $\phi$ . The covariant scheme for the charge correlator is compared with the RPA scheme and determinantal MC in the Hubbard model. The comparison demonstrates that the covariant scheme makes a significant improvement over the RPA scheme. The comparison of charge susceptibility demonstrates that the covariant scheme for charge correlator is consistent with the charge susceptibility, whereas the RPA calculation has a significant deviation.

The  $HGW$  method (to calculate the one - body Green's function) has a small complexity (for details, see Appendix E), and thus can be applied to large systems. The formalism presented in this paper is easily extended to more general cases, such as multi - orbital lattice models, as long as the band index is put in the generalized coordinate. The similarity to the traditional  $GW$  method helps the application of the  $HGW$  method to studying the electronic properties of realistic correlated materials. The substantial improvement over the  $GW$  method in relatively strong

coupling regime might imply that the *HGW* method is a good alternative in certain cases. However, the numerical cost of the calculation of the charge - conserving charge correlators is too large for realistic systems.

To fully study the Hubbard model, the spin channel is important, whereas neglected in our current formalism (the traditional *GW* method also neglects the spin channel). The variant of *GW* method including spin channel were proposed for example in Ref.[37–39]. The variant of *HGW* approximation could also be proposed by including spin channel to better account the spin fluctuation at strong fluctuation regime in the 2D Hubbard model in future research.

The self consistency is important to non - perturbative analytical methods, and numerous ideas are put forward to ensure several identities. For example, in the two - particle self - consistent (TPSC) theory [40–42], several “constants” are determined by the sum rules and identities. In contrast, the idea of the covariance is natural and universal in a sense that the correlators and the sum rules are treated in the same footing.

## ACKNOWLEDGMENTS

This work is supported by High-performance Computing Platform of Peking University. B.R. was supported by MOST of Taiwan, Grants No. 107-2112-M-003-023-MY3. D.P.L. was supported by National Natural Science Foundation of China, Grants No. 11674007 and No. 91736208. B.R. and D.P.L. are grateful to School of Physics of Peking University and The Center for Theoretical Sciences of Taiwan for hospitality, respectively.

### Appendix A: Dyson - Schwinger equations and Ward identities

#### 1. Dyson-Schwinger equations of motion

The invariance of the functional integral measure  $\mathcal{D}[\psi, \psi^*]$  under the infinitesimal variation of field  $\psi, \psi^*$  yields the equality [43]

$$\int \mathcal{D}[\psi, \psi^*] \frac{\delta}{\delta \psi^*(2)} \left( \psi^*(1) e^{-S[\psi, \psi^*; \phi]} \right) = 0. \quad (\text{A1})$$

Substituting the perturbed action (2) into the equality, one obtains the Dyson - Schwinger equation of motion:

$$\delta(1, 2) = \int d(3) T(1, 3) G(3, 2) + \phi(1) G(1, 2) - \int d(3) V(1, 3) G_2(1, 2; 3, 3). \quad (\text{A2})$$

Here the two - body correlator is defined by

$$\begin{aligned} G_2(1, 2; 3, 4) &\equiv \langle \psi^*(2) \psi(1) \psi^*(4) \psi(3) \rangle \\ &= \frac{1}{Z[\phi]} \int \mathcal{D}[\psi, \psi^*] \psi^*(2) \psi(1) \psi^*(4) \psi(3) e^{-S[\psi, \psi^*; \phi]}. \end{aligned} \quad (\text{A3})$$

Through the definition (4), one obtains the derivative of  $G$  with respect to  $\phi$ :

$$L(1, 2; 3) \equiv \frac{\delta G(1, 2)}{\delta \phi(3)} = G_2(1, 2; 3, 3) - G(1, 2) \rho(3), \quad (\text{A4})$$

where  $\rho(1) \equiv \langle \rho(1) \rangle = G(1, 1)$ . By virtue of Eq.(A4), one can express  $G_2$  in terms of  $G$  and  $\delta G/\delta \phi$ , and thus can obtain Eq.(5) from Eq.(A2).

#### 2. Ward identities for correlators

The invariance of the functional integral measure  $\mathcal{D}[\psi, \psi^*]$  under the infinitesimal phase rotation of the complex field  $\psi$  yields an equality [43]

$$\int \mathcal{D}[\psi, \psi^*] \left( \psi^*(1) \frac{\delta}{\delta \psi^*(1)} - \psi(1) \frac{\delta}{\delta \psi(1)} \right) e^{-S[\psi, \psi^*; \phi]} = 0. \quad (\text{A5})$$

Substituting the perturbed action (2), one obtains the Ward identity for Green's function  $G$ :

$$\int d(2) T(1,2) G(2,1) - T(2,1) G(1,2) = 0. \quad (\text{A6})$$

The derivative of Eq.(A6) with respect to  $\phi$  yields:

$$\int d(2) T(1,2) L(2,1;3) - T(2,1) L(1,2;3) = 0. \quad (\text{A7})$$

Eq.(A7) is the Ward identity for the two - body correlator  $L$ .

## Appendix B: Details of deriving $HGW$ equations and covariant $HGW$ equations

### 1. Derivation of $HGW$ equations

The  $HGW$  equations are derived from Eqs.(5, 11). First, one makes derivative of Eqs.(6, 7) with respect to  $\phi$ , and obtains

$$\frac{\delta H^{-1}(1,2)}{\delta \phi(3)} = \delta(1,2) \frac{\delta v(1)}{\delta \phi(3)}, \quad (\text{B1})$$

and

$$\frac{\delta v(1)}{\delta \phi(2)} = \delta(1,2) - \int d(3) V(1,3) \frac{\delta \rho(3)}{\delta \phi(2)}. \quad (\text{B2})$$

Substituting Eq.(B1) into Eq.(11) leads to

$$\frac{\delta G(1,2)}{\delta \phi(3)} = - \int d(4) H(1,4) G(4,2) \frac{\delta v(4)}{\delta \phi(3)}. \quad (\text{B3})$$

Plugging Eq.(B3) into Eq.(B2), and one obtains

$$\frac{\delta v(1)}{\delta \phi(2)} = \delta(1,2) + \int d(34) V(1,3) \Pi(3,4) \frac{\delta v(4)}{\delta \phi(2)}, \quad (\text{B4})$$

with

$$\Pi(1,2) \equiv H(1,2) G(2,1). \quad (\text{B5})$$

Then substituting Eq.(B3) into Eq.(5), one obtains

$$\delta(1,2) = \int d(3) H^{-1}(1,3) G(3,2) + \int d(34) V(1,3) H(1,4) G(4,2) \frac{\delta v(4)}{\delta \phi(3)}. \quad (\text{B6})$$

The equation above can be rewritten as

$$G^{-1}(1,2) = H^{-1}(1,2) - \Sigma(1,2), \quad (\text{B7})$$

with the self - energy function  $\Sigma$  given by

$$\Sigma(1,2) \equiv -H(1,2) W(2,1), \quad (\text{B8})$$

and the screened dynamical potential  $W$  defined by

$$W(1,2) \equiv \int d(3) \frac{\delta v(1)}{\delta \phi(3)} V(2,3). \quad (\text{B9})$$

Combining Eqs.(B4, B9), one arrives at the following equation

$$W(1,2) = V(1,2) + \int d(34) V(1,3) \Pi(3,4) W(4,2), \quad (\text{B10})$$

which can be rewritten as

$$W^{-1}(1,2) = V^{-1}(1,2) - \Pi(1,2). \quad (\text{B11})$$

Now four important equations (B5, B7, B8, B11) are derived and they are called the  $HGW$  equations.

## 2. Derivation of covariant $HGW$ equations

Here, details of derivation of covariant  $HGW$  equations are given. For convenience, one can introduce the covariant versions of two vertex functions:

$$\Lambda(1, 2; 3) \equiv \left. \frac{\delta G^{-1}(1, 2)}{\delta v(3)} \right|_{\phi=0}, \quad (\text{B12})$$

and

$$\Gamma(1, 2; 3) \equiv \left. \frac{\delta W^{-1}(1, 2)}{\delta v(3)} \right|_{\phi=0}. \quad (\text{B13})$$

The derivatives of  $HGW$  equations with respect to  $v$  can be easily obtained

$$\Lambda(1, 2; 3) = \frac{\delta H^{-1}(1, 2)}{\delta v(3)} + \frac{\delta H(1, 2)}{\delta v(3)} W(2, 1) + H(1, 2) \frac{\delta W(2, 1)}{\delta v(3)}, \quad (\text{B14})$$

$$\Gamma(1, 2; 3) = -\frac{\delta H(1, 2)}{\delta v(3)} G(2, 1) - H(1, 2) \frac{\delta G(2, 1)}{\delta v(3)}, \quad (\text{B15})$$

There is a general relation for an array  $X$ :

$$\frac{\delta X(1, 2)}{\delta v(3)} = -\int d(45) X(1, 4) X(5, 2) \frac{\delta X^{-1}(4, 5)}{\delta v(3)}, \quad (\text{B16})$$

and for  $X = H$ ,

$$\frac{\delta H^{-1}(1, 2)}{\delta v(3)} = \delta(1, 2) \delta(1, 3). \quad (\text{B17})$$

Then one can obtain the equation for  $\Lambda$

$$\begin{aligned} \Lambda(1, 2; 3) &= \delta(1, 2) \delta(1, 3) - H(1, 3) H(3, 2) W(2, 1) \\ &\quad - \int d(45) H(1, 2) W(2, 5) W(4, 1) \Gamma(5, 4; 3), \end{aligned} \quad (\text{B18})$$

and the equation for  $\Gamma$

$$\begin{aligned} \Gamma(1, 2; 3) &= H(1, 3) H(3, 2) G(2, 1) \\ &\quad + \int d(45) H(1, 2) G(2, 5) G(4, 1) \Lambda(5, 4; 3). \end{aligned} \quad (\text{B19})$$

From Eqs (B18, B19), one can obtain  $\Lambda$  and  $\Gamma$ , giving  $H, G, W$  obtained from on-shell ( $\phi = 0$ )  $HGW$  equations.

One can introduce  $\chi_0$  as

$$\chi_0(1, 2) \equiv \left. \frac{\delta \rho(1)}{\delta v(2)} \right|_{\phi=0}, \quad (\text{B20})$$

and then obtains Eq.(18). With the definitions (16, B20), one obtains

$$\chi^{\text{cov}}(1, 2) = \int d(3) \chi_0(1, 3) \frac{\delta v(3)}{\delta \phi(2)}. \quad (\text{B21})$$

By virtue of Eq.(B2), Eq.(B21) leads to Eq.(17).

## Appendix C: *HGW* and covariant *HGW* equations for the Hubbard model

### 1. Generalized Fourier transformation for the Hubbard model

The generalized Fourier transformation for the Hubbard model is introduced here. For a short formulation, two useful notations

$$\mathcal{E}_F(\alpha, 1-2) \equiv e^{i\pi\eta_\alpha \cdot (\sigma_1 - \sigma_2)} e^{ik_\alpha \cdot (i_1 - i_2)} e^{i\pi(2m_\alpha + 1) \cdot (\tau_1 - \tau_2)}, \quad (C1)$$

$$\mathcal{E}_B(\alpha, 1-2) \equiv e^{i\pi\eta_\alpha \cdot (\sigma_1 - \sigma_2)} e^{ik_\alpha \cdot (i_1 - i_2)} e^{i\pi 2m_\alpha \cdot (\tau_1 - \tau_2)}, \quad (C2)$$

are introduced, where the label  $\alpha$  refers to  $\eta_\alpha, k_\alpha, m_\alpha$ . For a fermionic array  $X_F$  which is anti-periodic over Matsubara time, one can expand it as Fourier series:

$$X_F(1, 2) = \frac{1}{\mathcal{N}} \sum_{\alpha} \tilde{X}_F(\alpha) \mathcal{E}_F(\alpha, 1-2). \quad (C3)$$

Here  $\mathcal{N} = 2MN^2$ ,  $M$  is the number of time slices and  $N^2$  is the number of lattice sites.  $\sigma$  is quantified as 1 for spin-down and 0 for spin-up, and correspondingly  $\eta$  takes value of 0 or 1.  $i$  is the coordinate of lattice site, and  $k$  is the momentum in the first Brillouin zone.  $\tau \in [0, \beta]$  is the discrete Matsubara time, and  $m$  takes integral value from 0 to  $M-1$ . The summation  $\sum_{\alpha}$  is over all possible values of  $\alpha \equiv (\eta_\alpha, k_\alpha, m_\alpha)$ . Similarly, one can expand a bosonic array  $X_B$ , which is periodic over Matsubara time, as Fourier series:

$$X_B(1, 2) = \frac{1}{\mathcal{N}} \sum_{\alpha} \tilde{X}_B(\alpha) \mathcal{E}_B(\alpha, 1-2). \quad (C4)$$

The coefficient  $T$  in action (1) is anti-periodic over Matsubara time and thus is a fermionic array. Substitute Eq.(23) into the ansatz (C3), and one obtains

$$\tilde{T}(\alpha) = \Delta\tau \left( -\frac{1}{\Delta\tau} \left( e^{-i\pi(2m+1)/M} - 1 \right) - \varepsilon(k_\alpha) + \mu \right), \quad (C5)$$

with

$$\varepsilon(k) = -2t(\cos(k_x) + \cos(k_y)), \quad (C6)$$

for the 2D Hubbard model, with  $k \equiv (k_x, k_y)$ . The coefficient  $V$  is periodic over Matsubara time and thus is a bosonic array. Substituting Eq.(24) into the ansatz (C4), one obtains

$$\tilde{V}(\alpha) = \Delta\tau U (-1)^{\eta_\alpha}. \quad (C7)$$

From definitions (C1, C2), one can derive the following relations

$$\begin{aligned} \mathcal{E}_F(\alpha, 1-2) \mathcal{E}_F(\alpha, 2-3) &= \mathcal{E}_F(\alpha, 1-3), \\ \mathcal{E}_B(\alpha, 1-2) \mathcal{E}_B(\alpha, 2-3) &= \mathcal{E}_B(\alpha, 1-3), \\ \mathcal{E}_F(\alpha, 1-2) \mathcal{E}_B(\beta, 1-2) &= \mathcal{E}_F(\alpha + \beta, 1-2), \\ \mathcal{E}_B(\alpha, 1-2) \mathcal{E}_F(\beta, 1-2) &= \mathcal{E}_B(\alpha + \beta, 1-2), \\ \mathcal{E}_F(\alpha, 1-2) \mathcal{E}_F(\beta, 2-1) &= \mathcal{E}_B(\alpha - \beta, 1-2), \\ \mathcal{E}_B(\alpha, 1-2) &= \mathcal{E}_B(-\alpha, 2-1). \end{aligned} \quad (C8)$$

These equations are helpful in the derivation of *HGW* equations in Fourier space.

### 2. *HGW* equations for the Hubbard model

In *HGW* equations, one encounters with several quantities: the fermionic arrays  $H, G, \Sigma$  and the bosonic arrays  $W, \Pi$ . Substitute the ansatz (C3, C4) into the *HGW* equations, and one obtains the *HGW* equations in Fourier space

for the Hubbard model

$$\begin{aligned}
\tilde{G}^{-1}(\alpha) &= \tilde{H}^{-1}(\alpha) - \tilde{\Sigma}(\alpha), \\
\tilde{\Sigma}(\alpha) &= -\frac{1}{\mathcal{N}} \sum_{\gamma} \tilde{H}(\alpha + \gamma) \tilde{W}(\gamma), \\
\tilde{W}^{-1}(\alpha) &= \tilde{V}^{-1}(\alpha) - \tilde{\Pi}(\alpha), \\
\tilde{\Pi}(\alpha) &= \frac{1}{\mathcal{N}} \sum_{\gamma} \tilde{H}(\alpha + \gamma) \tilde{G}(\gamma),
\end{aligned} \tag{C9}$$

with

$$\tilde{H}^{-1}(\alpha) = \tilde{T}(\alpha) - \frac{2U}{\mathcal{N}} \sum_{\gamma} \tilde{G}(\gamma). \tag{C10}$$

### 3. Covariant *HGW* equations for the Hubbard model

Similarly, one can obtain the covariant *HGW* equations in Fourier space for the Hubbard model. One can make the ansatz for the vertex functions,

$$\Lambda(1, 2, 3) = \frac{1}{\mathcal{N}^2} \sum_{\alpha, \gamma} \tilde{\Lambda}(\alpha, \gamma) \mathcal{E}_F(\alpha, 1-2) \mathcal{E}_B(\gamma, 1-3), \tag{C11}$$

$$\Gamma(1, 2, 3) = \frac{1}{\mathcal{N}^2} \sum_{\alpha, \gamma} \tilde{\Gamma}(\alpha, \gamma) \mathcal{E}_B(\alpha, 1-2) \mathcal{E}_B(\gamma, 1-3). \tag{C12}$$

And one can obtain from Eqs.(B18, B19),

$$\begin{aligned}
\tilde{\Lambda}(\alpha, \beta) &= 1 - \frac{1}{\mathcal{N}} \sum_{\gamma} \tilde{H}(\alpha + \beta + \gamma) \tilde{H}(\alpha + \gamma) \tilde{W}(\gamma) \\
&\quad - \frac{1}{\mathcal{N}} \sum_{\gamma} \tilde{H}(\alpha + \beta + \gamma) \tilde{W}(\beta + \gamma) \tilde{W}(\gamma) \tilde{\Gamma}(\gamma, \beta),
\end{aligned} \tag{C13}$$

and

$$\begin{aligned}
\tilde{\Gamma}(\alpha, \beta) &= \frac{1}{\mathcal{N}} \sum_{\gamma} \tilde{H}(\alpha + \beta + \gamma) \tilde{H}(\alpha + \gamma) \tilde{G}(\gamma) \\
&\quad + \frac{1}{\mathcal{N}} \sum_{\gamma} \tilde{H}(\alpha + \beta + \gamma) \tilde{G}(\beta + \gamma) \tilde{G}(\gamma) \tilde{\Lambda}(\gamma, \beta).
\end{aligned} \tag{C14}$$

Combine Eqs.(C13, C14), and one obtains

$$\sum_{\gamma} \mathcal{M}(\alpha, \gamma, \beta) \tilde{\Lambda}(\gamma, \beta) = b(\alpha, \beta), \tag{C15}$$

with

$$\begin{aligned}
\mathcal{M}(\alpha, \gamma, \beta) &= \delta(\alpha, \gamma) + \frac{1}{\mathcal{N}} \tilde{G}(\beta + \gamma) \tilde{G}(\gamma) \\
&\quad \times \frac{1}{\mathcal{N}} \sum_{\lambda} \tilde{H}(\alpha + \beta + \lambda) \tilde{W}(\beta + \lambda) \tilde{W}(\lambda) \tilde{H}(\beta + \gamma + \lambda),
\end{aligned} \tag{C16}$$



and

$$\begin{aligned}
b(\alpha, \beta) = & 1 - \frac{1}{\mathcal{N}} \sum_{\gamma} \tilde{H}(\alpha + \beta + \gamma) \tilde{H}(\alpha + \gamma) \tilde{W}(\gamma) \\
& - \frac{1}{\mathcal{N}} \sum_{\gamma} \tilde{H}(\alpha + \beta + \gamma) \tilde{W}(\beta + \gamma) \tilde{W}(\gamma) \\
& \times \frac{1}{\mathcal{N}} \sum_{\lambda} \tilde{H}(\beta + \gamma + \lambda) \tilde{H}(\gamma + \lambda) \tilde{G}(\lambda).
\end{aligned} \tag{C17}$$

Once Eq.(C15) is solved,  $\tilde{\Lambda}$  will be obtained.

Next, one can make ansatz

$$\chi_0(1, 2) = \frac{1}{\mathcal{N}} \sum_{\alpha} \tilde{\chi}_0(\alpha) \mathcal{E}_B(\alpha, 1-2), \tag{C18}$$

$$\chi^{\text{cov}}(1, 2) = \frac{1}{\mathcal{N}} \sum_{\alpha} \tilde{\chi}^{\text{cov}}(\alpha) \mathcal{E}_B(\alpha, 1-2). \tag{C19}$$

Then Eq.(18) yields

$$\tilde{\chi}_0(\alpha) = - \sum_{\gamma} \tilde{G}(\alpha + \gamma) \tilde{G}(\gamma) \tilde{\Lambda}(\gamma, \alpha), \tag{C20}$$

and Eq.(17) yields

$$\tilde{\chi}^{\text{cov}}(\alpha) = \frac{\tilde{\chi}_0(\alpha)}{1 + \tilde{V}(\alpha) \tilde{\chi}_0(\alpha)}. \tag{C21}$$

Up to now, the covariant *HGW* equations (C15, C20, C21) are obtained in Fourier space for the Hubbard model.

#### Appendix D: Correlators in Matsubara action

The Matsubara action given in (22) is dependent of the number of time slices  $M$ , and tends to the continuous time limit

$$S[\psi, \psi^*] = \sum_{i, \sigma} \int_0^{\beta} d\tau \psi_{i, \sigma}^*(\tau) \partial_{\tau} \psi_{i, \sigma}(\tau) + \int_0^{\beta} d\tau \mathcal{H}[\psi_{i\sigma}^*(\tau), \psi_{i\sigma}(\tau)], \tag{D1}$$

with a convergence speed  $1/M$ . For a short formulation, the spin and space coordinates are dropped below. One can define the  $M$ -dependent Green's function as

$$G_M(\tau_{l_1}, \tau_{l_2}) \equiv \frac{1}{Z_M} \int \mathcal{D}[\psi, \psi^*] \psi^*(\tau_{l_2}) \psi(\tau_{l_1}) e^{-S_M[\psi, \psi^*]}, \tag{D2}$$

with the partition function

$$Z_M \equiv \int \mathcal{D}[\psi, \psi^*] e^{-S_M[\psi, \psi^*]}. \tag{D3}$$

Since as  $M$  tends to infinity,  $S_M[\psi, \psi^*]$  tends to  $S[\psi, \psi^*]$  with a convergence speed  $\frac{1}{M}$ , then  $G_M(\tau_{l_1}, \tau_{l_2})$  tends to  $G(l_1\beta/M, (l_2+1)\beta/M)$  with the same convergence speed. For this reason, one can approximate that in the continuous time limit

$$G\left(\frac{l_1}{M}\beta, \frac{l_2+1}{M}\beta\right) = 2G_{2M}(\tau_{2l_1}, \tau_{2l_2+1}) - G_M(\tau_{l_1}, \tau_{l_2}). \tag{D4}$$

Define the  $M$ -dependent particle density as

$$\rho_M(\tau_l) \equiv G_M(\tau_l, \tau_l). \quad (\text{D5})$$

As  $M$  tends to infinity, it tends to the particle density in continuous time limit. Then one can conclude that the  $M$ -dependent particle density  $\rho_M$  tends to the particle density  $\rho$  with a convergence speed  $1/M$  as  $M$  tends to infinity. Therefore, one can approximate that

$$\rho(l\beta/M) = 2\rho_{2M}(\tau_{2l}) - \rho_M(\tau_l). \quad (\text{D6})$$

Eqs.(D4, D6) help to lower down the error of  $O(1/M)$  caused by finite  $M$  to  $O(1/M^2)$ .

## Appendix E: Algorithm

### 1. Routine for the Green's function

The  $HGW$  equations (C9) are mathematically nonlinear equations of the Green's function  $\tilde{G}$ . To solve the nonlinear equations, one can use the Broyden algorithm [44]. The Broyden algorithm is designed to solve the non-linear equations  $F[X] = 0$  with an initial value  $X = X_0$ . This algorithm mainly contains two inputs, the nonlinear function  $F$ , and the initial value  $X_0$ . In our cases,  $X$  stands for the Green's function  $\tilde{G}$ , and  $F$  stands for  $\tilde{G}' - \tilde{G}$ , where  $\tilde{G}'$  is given by

$$\tilde{G}' = \frac{1}{\tilde{H}^{-1} + \mathcal{C} \left[ \tilde{H}, \frac{1}{\tilde{V}^{-1} - \mathcal{C}[\tilde{H}, \tilde{G}]} \right]}, \quad (\text{E1})$$

with the correlation functional

$$\mathcal{C}[\tilde{X}, \tilde{Y}](\alpha) \equiv \frac{1}{\mathcal{N}} \sum_{\gamma} \tilde{X}(\alpha + \gamma) \tilde{Y}(\gamma), \quad (\text{E2})$$

and  $X_0$  stands for the initial value given by

$$\tilde{G}_0(\alpha) = \frac{1}{T(\alpha) - \frac{U}{2}\rho_0 - \Sigma_0(\alpha)}, \quad (\text{E3})$$

where the initial particle density  $\rho_0 \in (0, 2)$  is given randomly, and the initial self energy  $\Sigma_0$  is also given randomly. Note that the correlation (E2) can be fasten by discrete Fourier transformation (DFT) algorithm [44], and as a result, the complexity of one iteration (E1) is  $\mathcal{O}(N \log N)$ .

There might be multiple solutions to the nonlinear equations. In our calculations, only one solution is found in the case that  $U/t$  is sufficiently small, or  $\beta t$  is sufficiently small. However, multiple solutions are found in the case of strongly coupling and low temperature. Our strategy is setting gradients to  $U$  or  $\beta$ , and then solving the Green's function with different initial values for each parameter, and finally choosing the solution continuous with  $U$  or  $\beta$ .

To eliminate the error of  $1/M$  of the Green's function in Matsubara time, one can set different numbers of Matsubara time slices, and then make extrapolation. In our calculations,  $M$  is set to 512, 1024 and 2048. To show  $M$  is sufficiently large, one can verify  $(2\rho_{2048} - \rho_{1024}) - (2\rho_{1024} - \rho_{512})$  is close to zero. To obtain the density, one can use the approximation  $\rho \doteq 2\rho_{2048} - \rho_{1024}$ . To obtain the Green's function, one uses

$$G\left(\frac{l_1}{1024}\beta, \frac{l_2+1}{1024}\beta\right) = 2G_{2048}(\tau_{2l_1}, \tau_{2l_2+1}) - G_{1024}(\tau_{l_1}, \tau_{l_2}). \quad (\text{E4})$$

Clearly, Green's function on only discrete Matsubara time can be obtained. In addition, the particle density  $n$  per site relates to  $\rho$  through the relation

$$n \equiv n_i(\tau) = \rho_{i\uparrow}(\tau) + \rho_{i\downarrow}(\tau). \quad (\text{E5})$$

The numerical cost of the calculation of the Green function is analyzed as follows. For  $U = 2, T = 0.125$  at half filling and  $M = 1024, N = 16$ , the typical numerical cost is about 2.3 seconds running on a 32 - core CPU(2.6GHz). The numerical cost is almost proportional to  $MN^2$ , and thus is applicable to complicated systems.

The parameters  $U$  and  $T$  influence the number of iterations, and then influence the numerical cost. We set  $M = 1024$  and  $N = 16$ . The numerical costs dependent on  $U$  at  $T = 0.125$  are presented in Tab.II, and the results demonstrate

that the numerical cost might be exponential in the Hubbard  $U$ . The numerical costs dependent on  $T$  at  $U = 2$  are presented in Tab.III, and the results demonstrate that the numerical cost is almost linear in  $1/T$ . Besides, for a good precision, one should increase  $M$  as  $U$  increases or  $T$  decreases. According to our experience, setting  $M = [16 \times U/T]$  yields a satisfactory precision (after the extrapolation (D4)). With these factors in consideration, the  $HGW$  method should be applicable to the cases at sufficiently low temperature but not very large  $U$ .

TABLE II. Dependence of the numerical cost on the Hubbard  $U$ 

$U$	2.0	2.5	3.0	3.5	4.0
cost (seconds)	2.257	5.919	7.743	16.429	38.945

TABLE III. Dependence of the numerical cost on the inverse temperature

$1/T$	8.0	16.0	24.0	32.0
cost (seconds)	2.367	3.523	7.497	10.967

## 2. Routine for the density - density correlator

In the routine for the density - density correlator, there are mainly three steps. First, calculate  $\tilde{H}, \tilde{W}$  for given  $\tilde{G}$  and parameters. Second, construct  $\mathcal{M}$  and  $b$ , and solve the linear equations (C15) to obtain  $\tilde{\Lambda}$ . Third, calculate  $\tilde{\chi}_0$  using Eq.(C20), and calculate  $\tilde{\chi}^{\text{cov}}$  using Eq.(C21). The second step has the largest complexity, up to  $\mathcal{O}(N^4)$ . The linear equations can be solved iteratively in a much faster speed than the linear system solver.

The charge correlator  $\chi^{\text{ch}}$  relates to  $\chi$  through the relation

$$\begin{aligned} \chi_{i_1, i_2}^{\text{ch}}(\tau_1, \tau_2) &\equiv \langle n_{i_1}(\tau_1) n_{i_2}(\tau_2) \rangle - \langle n_{i_1}(\tau_1) \rangle \langle n_{i_2}(\tau_2) \rangle \\ &= \sum_{\sigma_1, \sigma_2} \chi_{i_1 \sigma_1, i_2 \sigma_2}(\tau_1, \tau_2). \end{aligned} \quad (\text{E6})$$

Note that

$$\chi_{i_1 \sigma_1, i_2 \sigma_2}(\tau_1, \tau_2) = \langle \rho_{i_1 \sigma_1}(\tau_1) \rho_{i_2 \sigma_2}(\tau_2) \rangle - \langle \rho_{i_1 \sigma_1}(\tau_1) \rangle \langle \rho_{i_2 \sigma_2}(\tau_2) \rangle. \quad (\text{E7})$$

The charge susceptibility  $\chi_c \equiv \partial n / \partial \mu$  in discrete time Matsubata action should satisfy

$$\chi_c = \Delta\tau \sum_{l=0}^{M-1} \sum_i \langle n m_i(\tau_l) \rangle_c = \Delta\tau \tilde{\chi}^{\text{ch}}(0, 0), \quad (\text{E8})$$

with the (discrete) Fourier transformation

$$\chi_{i_1 i_2}^{\text{ch}}(\tau_1, \tau_2) = \frac{1}{MN^2} \sum_{k, m} \tilde{\chi}^{\text{ch}}(k, m) e^{ik \cdot (i_1 - i_2)} e^{i\pi 2m \cdot (\tau_1 - \tau_2)}. \quad (\text{E9})$$

The numerical cost of calculation of the two - body correlators is analyzed as follows. For  $M = 1024, N = 4$ , the typical numerical cost is about 3 hours running on a 32 - core CPU(2.6GHz). The numerical cost is almost proportional to the square of  $MN^2$ , and is almost independent of  $U$  and  $T$ . The numerical cost is a bit large, and is not applicable to realistic materials with the current algorithm.

## Appendix F: $GW$ equations

The  $GW$  approximation is based on Hedin's equations

$$\begin{aligned} G^{-1}(1, 2) &= H^{-1}(1, 2) - \Sigma(1, 2), \\ \Sigma(1, 2) &= - \int d(34) G(1, 4) W(3, 1) \Lambda(4, 2; 3), \\ W^{-1}(1, 2) &= V^{-1}(1, 2) - \Pi(1, 2), \\ \Pi(1, 2) &= \int d(34) G(1, 3) G(4, 1) \Lambda(3, 4; 2), \end{aligned} \quad (\text{F1})$$

with Hedin's vertex  $\Lambda(1, 2; 3) = \delta G^{-1}(1, 2)/\delta v(3)$ .

One can make the simplest approximation for Hedin's vertex  $\Lambda$ ,

$$\Lambda(1, 2; 3) \doteq \delta H^{-1}(1, 2)/\delta v(3) = \delta(1, 2)\delta(1, 3),$$

to obtain the *GW* equations

$$\begin{aligned} G^{-1}(1, 2) &= H^{-1}(1, 2) - \Sigma(1, 2), \\ \Sigma(1, 2) &= -G(1, 2)W(2, 1), \\ W^{-1}(1, 2) &= V^{-1}(1, 2) - \Pi(1, 2), \\ \Pi(1, 2) &= G(1, 2)G(2, 1). \end{aligned} \tag{F2}$$

- 
- [1] M. Imada, A. Fujimori, and Y. Tokura, Metal-insulator transitions, *Reviews of Modern Physics* **70**, 1039 (1998).
- [2] A. Auerbach, *Interacting Electrons and Quantum Magnetism* (Springer Science & Business Media, 2012).
- [3] T. Timusk and B. Statt, The pseudogap in high-temperature superconductors: an experimental survey, *Reports on Progress in Physics* **62**, 61 (1999).
- [4] P. A. Lee, N. Nagaosa, and X. G. Wen, Doping a Mott insulator: Physics of high-temperature superconductivity, *Reviews of Modern Physics* **78**, 17 (2006).
- [5] E. Dagotto, Correlated Electrons in High-Temperature Superconductors, *Reviews of Modern Physics* **66**, 763 (1994).
- [6] D. J. Scalapino, A common thread: The pairing interaction for unconventional superconductors, *Reviews of Modern Physics* **84**, 1383 (2012).
- [7] J. Hubbard, Electron Correlations in Narrow Energy Bands, *Proceedings of the Royal Society of London Series a-Mathematical and Physical Sciences* **276**, 238 (1963).
- [8] U. Schollwöck, The density-matrix renormalization group, *Reviews of Modern Physics* **77**, 259 (2005).
- [9] F. Becca and S. Sorella, *Quantum Monte Carlo Approaches for Correlated Systems* (Cambridge University Press, Cambridge, 2017).
- [10] A. Georges, G. Kotliar, W. Krauth, and M. J. Rozenberg, Dynamical mean-field theory of strongly correlated fermion systems and the limit of infinite dimensions, *Reviews of Modern Physics* **68**, 13 (1996).
- [11] G. Kotliar, S. Y. Savrasov, K. Haule, V. S. Oudovenko, O. Parcollet, and C. A. Marianetti, Electronic structure calculations with dynamical mean-field theory, *Reviews of Modern Physics* **78**, 865 (2006).
- [12] G. Rohringer, H. Hafermann, A. Toschi, A. A. Katanin, A. E. Antipov, M. I. Katsnelson, A. I. Lichtenstein, A. N. Rubtsov, and K. Held, Diagrammatic routes to nonlocal correlations beyond dynamical mean field theory, *Rev. Mod. Phys.* **90**, 025003 (2018).
- [13] T. Schäfer, N. Wentzell, F. Simkovic, Y.-Y. He, C. Hille, M. Klett, C. J. Eckhardt, B. Arzhang, V. Harkov, F.-M. Le Regent, A. Kirsch, Y. Wang, A. J. Kim, E. Kozik, E. A. Stepanov, A. Kauch, S. Andergassen, P. Hansmann, D. Rohe, Y. M. Vilch, J. P. F. LeBlanc, S. Zhang, A. M. S. Tremblay, M. Ferrero, O. Parcollet, and A. Georges, Tracking the footprints of spin fluctuations: A multimethod, multimessenger study of the two-dimensional hubbard model, *Phys. Rev. X* **11**, 011058 (2021).
- [14] G. Baym and L. Kadanoff, Conservation Laws and Correlation Functions, *Physical Review* **124**, 287 (1961).
- [15] G. Baym, Self-Consistent Approximations in Many-Body Systems, *Physical Review* **127**, 1391 (1962).
- [16] L. Hedin, New Method for Calculating the One-Particle Green's Function with Application to the Electron-Gas Problem, *Physical Review* **139**, A796 (1965).
- [17] C. Dedominicis and P. Martin, Stationary Entropy Principle + Renormalization in Normal + Superfluid Systems .2. Diagrammatic Formulation, *Journal of Mathematical Physics* **5**, 31 (1964).
- [18] L. Kadanoff and P. Martin, Theory of Many-Particle Systems .2. Superconductivity, *Physical Review* **124**, 670 (1961).
- [19] Q. J. Chen, J. Stajic, S. Tan, and K. Levin, BCS-BEC crossover: From high temperature superconductors to ultracold superfluids, *Physics Reports-Review Section of Physics Letters* **412**, 1 (2005).
- [20] B. Rosenstein and D. Li, Covariant cubic approximation for many-body electronic systems, *Physical Review B* **98**, 155126 (2018).
- [21] F. Aryasetiawan and O. Gunnarsson, The GW method, *Reports on Progress in Physics* **61**, 237 (1998).
- [22] N. E. Bickers, D. J. Scalapino, and S. R. White, Conserving approximations for strongly correlated electron systems: Bethe-salpeter equation and dynamics for the two-dimensional hubbard model, *Phys. Rev. Lett.* **62**, 961 (1989).
- [23] C. Dedominicis and P. Martin, Stationary Entropy Principle + Renormalization in Normal + Superfluid Systems .i. Algebraic Formulation, *Journal of Mathematical Physics* **5**, 14 (1964).
- [24] N. E. Bickers and S. R. White, Conserving approximations for strongly fluctuating electron systems. II. Numerical results and parquet extension, *Physical Review B* **43**, 8044 (1991).
- [25] Z. Fan, Z. Sun, D. Li, I. Berenstein, G. Leshem, and B. Rosenstein, Covariant Bethe-Salpeter approximation in models of strongly correlated electron systems, *Physical Review E* **101**, 023310 (2020).

- [26] A. L. Kutepov and G. Kotliar, One-electron spectra and susceptibilities of the three-dimensional electron gas from self-consistent solutions of Hedin's equations, *Physical Review B* **96**, 035108 (2017).
- [27] K. Morita, H. Maebashi, and K. Miyake, FLEX study on the compressibility of the two-dimensional Hubbard model, *Physica B-Condensed Matter* **312**, 547 (2002).
- [28] A. Kovner and B. Rosenstein, Covariant Gaussian Approximation .1. Formalism, *Physical Review D* **39**, 2332 (1989).
- [29] B. Rosenstein and A. Kovner, Covariant Gaussian Approximation .2. Scalar Theories, *Physical Review D* **40**, 504 (1989).
- [30] J. F. Wang, D. P. Li, H. C. Kao, and B. Rosenstein, Covariant gaussian approximation in Ginzburg-Landau model, *Annals of Physics* **380**, 228 (2017).
- [31] J. W. Negele, *Quantum Many-particle Systems* (CRC Press, 2018).
- [32] J. Fei, C.-N. Yeh, and E. Gull, Nevanlinna analytical continuation, *Phys. Rev. Lett.* **126**, 056402 (2021).
- [33] N. Bulut, D. J. Scalapino, and S. R. White, One-electron spectral weight of the doped two-dimensional hubbard model, *Phys. Rev. Lett.* **72**, 705 (1994).
- [34] A. Tanaka, Metal-insulator transition in the two-dimensional hubbard model: Dual fermion approach with lanczos exact diagonalization, *Phys. Rev. B* **99**, 205133 (2019).
- [35] B. Kyung, G. Kotliar, and A.-M. S. Tremblay, Quantum monte carlo study of strongly correlated electrons: Cellular dynamical mean-field theory, *Phys. Rev. B* **73**, 205106 (2006).
- [36] D. Sénéchal, D. Perez, and M. Pioro-Ladrière, Spectral weight of the hubbard model through cluster perturbation theory, *Phys. Rev. Lett.* **84**, 522 (2000).
- [37] T. Ayrál and O. Parcollet, Mott physics and spin fluctuations: A unified framework, *Phys. Rev. B* **92**, 115109 (2015).
- [38] T. Ayrál and O. Parcollet, Mott physics and spin fluctuations: A functional viewpoint, *Phys. Rev. B* **93**, 235124 (2016).
- [39] J. Vucicevic, T. Ayrál, and O. Parcollet, TRILEX and GW plus EDMFT approach to d-wave superconductivity in the Hubbard model, *Physical Review B* **96**, 104504 (2017).
- [40] Y. Vilk and A.-M. Tremblay, Non-perturbative many-body approach to the hubbard model and single-particle pseudogap, *Journal de Physique I* **7**, 1309 (1997).
- [41] H. Miyahara, R. Arita, and H. Ikeda, Development of a two-particle self-consistent method for multiorbital systems and its application to unconventional superconductors, *Phys. Rev. B* **87**, 045113 (2013).
- [42] K. Zantout, S. Backes, and R. Valentí, Two-particle self-consistent method for the multi-orbital hubbard model, *Annalen der Physik* **533**, 2000399 (2021).
- [43] M. Peskin, *An introduction to quantum field theory* (CRC press, 2018).
- [44] W. H. Press, S. A. Teukolsky, W. T. Vetterling, and B. P. Flannery, Numerical recipes in C++, *The art of scientific computing* **2**, 1002 (1992).